Electric fields enable tunable surfactant transport to microscale fluid interfaces

Rajarshi Sengupta, Aditya S. Khair, and Lynn M. Walker*
Department of Chemical Engineering, Carnegie Mellon University, Pittsburgh, Pennsylvania 15213, USA

(Received 23 April 2019; published 23 August 2019)

The transport dynamics of oil-soluble surfactants to oil-water interfaces are quantified using a custom-built electrified capillary microtensiometer platform. Dynamic interfacial tension measurements reveal that surfactant transport is enhanced under a dc electric field, due to electro-migration of charge carriers in the oil toward the interface. Notably, this enhancement can be precisely tuned by altering the field strength and temporal scheduling. We demonstrate electric fields as a new parameter to manipulate surfactant transport to microscale fluid-fluid interfaces.

DOI: 10.1103/PhysRevE.100.023114

I. INTRODUCTION

Electric fields act across fluid-fluid interfaces in electrocoalescence [1,2], inkjet printing [3,4], electroemulsification [5–7], and microfluidic devices [8–11]. These systems typically consist of drops of one fluid dispersed in another, with surfactants adsorbing from the bulk phases to the interface. Electric fields give rise to stresses at the interface. Depending on the strength of the field, the interface may attain a deformed steady shape or undergo an instability to form smaller drops. Interface deformation, and mechanisms of instability for systems of pure fluids, i.e., without added surfactant, has been well characterized [12–21]. The limited existing work on the deformation of surfactant-laden interfaces under electric fields is restricted to experiments and computations to predict drop deformation and breakup [22–27]. An inherent assumption in the computations is that the surfactant is insoluble; therefore, the effect of electric field on surfactant transport from bulk to the interface is not accounted for.

Surfactant transport from bulk to a fluid-fluid interface in the absence of electric field follows two transport processes [28,29]. Bulk surfactant diffuses to the interface (diffusion), and surfactant near the interface undergoes adsorption (desorption) to (from) from the interface (kinetic). The transport is known to be a function of bulk concentration, isotherm, local convection, and interface geometry [30–36]. However, the impact of electric fields has not been determined. For oil-water interfaces, the electric field acts almost solely in the oil phase because the electrical conductivity of deionized water is nearly $\mathcal{O}(10^6)$ larger than most oils. Surfactants are frequently added to oils and nonpolar liquids in several applications. For example, OLOA 11000, a polyisobutylene succinimide surfactant, is added to motor oil to prevent soot formation in internal combustion engines, disperse pigments in oils for use in electrophoretic displays, and even to prevent sparking during pumping of oils [37–39]. The addition of surfactants to oils has been observed to increase the electrical conductivity, both below and above the critical micellar concentration (CMC), even when the surfactant is considered nonionic [39–41]. It is hypothesized that below the CMC surfactant molecules form complexes with ionic impurities in oil, which acquire charge by disproportionation [40]. An electric field will exert a force on these charged species and could influence their bulk transport. Thus, the first step to accurately predict the deformation and breakup of surfactant-laden interfaces under electric fields is to determine whether bulk surfactant transport couples with electric fields.

Here we present novel experiments to quantify the transport of oil-soluble surfactants to oil-water interfaces using a microscale capillary tensiometer platform, under a dc electric field. Dynamic interfacial tension was measured under different electric field strengths to determine the rate of surfactant transport to the interface. We show that for a system whose electrical conductivity increases on addition of surfactant, the transport is enhanced under electric fields. The rate of surfactant transport can be manipulated by tuning the strength of the electric field. On the contrary, a system whose electrical conductivity is unaffected by surfactant addition does not show any coupling of surfactant transport with electric field.

II. MATERIALS AND METHODS

The surfactants chosen were a polyisobutylene succinimide surfactant, commercially known as OLOA 11000, donated by Chevron Oronite (San Ramon, CA), and a polyethylene-polypropylene block copolymer, Pluronic L64, purchased from BASF. The surfactants were reported to have a molecular weight of 950 and 2900 g/mol, respectively. Stock solutions of 0.62 mM OLOA was prepared in Isopar-M, an alkane mixture purchased from Exxon Mobil, and 3.71 mM Pluronic was prepared in 100 cSt silicone oil, purchased from Gelest, Inc. The stock solutions were diluted to different concentrations for the experiments. Deionized water was taken from a Barnstead UV Ultrapure II purification system (resistivity of 18.2 MΩ cm).

The experimental setup is an electrified version of the microtensiometer platform described in Ref. [35]. The schematic is shown in Fig. 1, with gravity pointing into the plane of the

*lwalker@andrew.cmu.edu

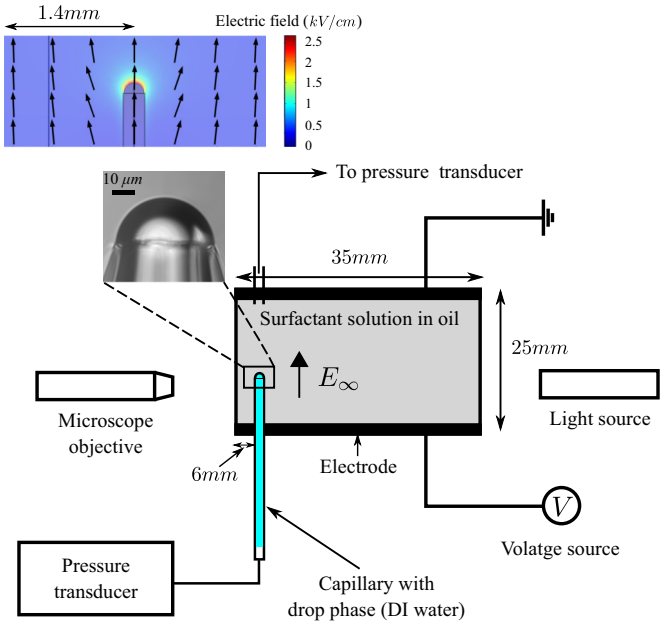

FIG. 1. Schematic of the experimental setup. Top left inset shows COMSOL simulations of electric field lines around a capillary of diameter 70 μm.

paper. Surfactant solution is filled in a cell of rectangular cross section (35 mm × 25 mm), three-dimensional printed using an acrylic material. Two electrodes are attached to opposite walls of the cell, 25 mm apart. Voltages in the range 0.1–2 kV were applied using a voltage source, setting electric fields ∼0.04–0.8 kV/cm across the cell. The electrodes have a hole of diameter 6 mm drilled through them. A glass capillary containing deionized water is inserted through one of the walls of the cell and one electrode. All capillaries used were pulled using a micropipette puller to diameters ∼70–80 μm. The capillary is connected to a differential pressure transducer, with the other end connected to the opposite wall of the cell. The other two walls have glass windows to enable viewing of the interface, which is imaged using a camera attached to a Nikon microscope objective lens (20×), and a radius fitted using a Labview routine. The capillary is inserted 6 mm away from the wall near the camera. COMSOL simulations predict the electric field lines to be unaffected by the wall when the gap between the wall and the capillary is more than 20 capillary radii. This chosen distance ensures that the capillary is within the field of view of the microscope objective, and field lines are not affected by the cell wall.

Surfactant transport is quantified by the dynamic interfacial tension, γ, of the interface. This is obtained from the instantaneous measurement of the radius of curvature of the hemispherical interface, R, and the pressure jump across the interface, ΔP, using the Young-Laplace equation, $\gamma = \Delta P \times R/2$. The interface is maintained at a constant pressure head, and the change in interfacial tension is primarily accounted for by the change in radius of curvature of the interface. Under electric fields, the Laplace equation will have an additional contribution from electric (Maxwell) stresses acting at the interface, which scale as $\epsilon_o E_\infty^2$, where ϵ_o is the permittivity of the oil, and E_∞ is the field strength. The scaled stress balance equation at the interface assumes the form $\Delta P/(\gamma/R) = 2 + \mathrm{Ca}_E \Delta T_E$, where $\mathrm{Ca}_E = R\epsilon_o E_\infty^2/\gamma$ is the electric capillary number, and ΔT_E is the dimensionless electric stress jump across the interface. For all field strengths and interface radii, $\mathrm{Ca}_E < \mathcal{O}(10^{-4})$. Thus, electric stresses were ignored while calculating the dynamic interfacial tension. The low Ca_E also ensured that the interface remained hemispherical at all field strengths studied.

III. RESULTS AND DISCUSSION

The principle of the instrument has been previously used to characterize transport of surfactants from water to air-water [35,36] and oil-water interfaces [42,43], with the aqueous surfactant solution in the cell. Here we have the oil-soluble surfactant in the cell and water in the capillary and quantify surfactant transport from the oil phase to the oil-water interface. The interfacial tension of pure Isopar-water was measured to be 52.5 ± 0.3, which is typical of alkane-water interfaces [42] and that of silicone oil-water was 40.3 ± 0.4 mN/m, in agreement with reported values [44]. Under an applied electric field, the interfacial tension was not observed to change beyond the error of the instrument (1 mN/m) for field strengths used in this study.

The transport and adsorption of OLOA in Isopar was measured to the Isopar-water interface at two different surfactant concentrations (4 and 10 μM) under different electric field strengths. A new interface was formed by subjecting the drop phase in the capillary to a high-pressure head using a solenoid valve. For a newly formed interface, the interfacial tension starts decreasing from the clean interfacial tension value and relaxes to a steady state of 26.2 ± 0.3 mN/m for the 4 μM system and 22.9 ± 0.3 mN/m for the 10 μM system. The system is deduced to reach steady state when the interfacial tension does not change by more than 1 mN/m for at least 1000 s. The dynamic interfacial tension of the 4 μM system is shown in Fig. 2(a). For the experiments, data were collected at each millisecond; however, for clarity, we show 50 data points spaced equally on a logarithmic scale in the figure. The inset shows the dynamic interfacial tension for the last 1000 s under each electric field, with a shifted time axis, on a linear scale. Surfactant transport is known to depend on the radius of curvature of the interface [35]. In all the experiments, the pressure head was held constant at the same value, ensuring the initial radius of curvature for all the interfaces differed by <5 μm. It follows that the time to reach steady state decreases with increasing values of the electric field. Under a field of 0.4 kV/cm, the system reaches steady state nearly 4 times faster than under no applied field. The effect is more prominent at lower values of the electric field. Dynamic interfacial tension curves for 0.2 and 0.4 kV/cm nearly overlap with each other, having slightly faster dynamics under 0.4 kV/cm. All the curves reach the same steady-state interfacial tension, indicated by the dashed line and depicted in the inset. This suggests that the electric field has negligible effect on the adsorption isotherm. The dynamic interfacial tension for 10 μM OLOA showed a similar trend. Evidently, the transport of OLOA to the Isopar-water interface is enhanced under electric fields.

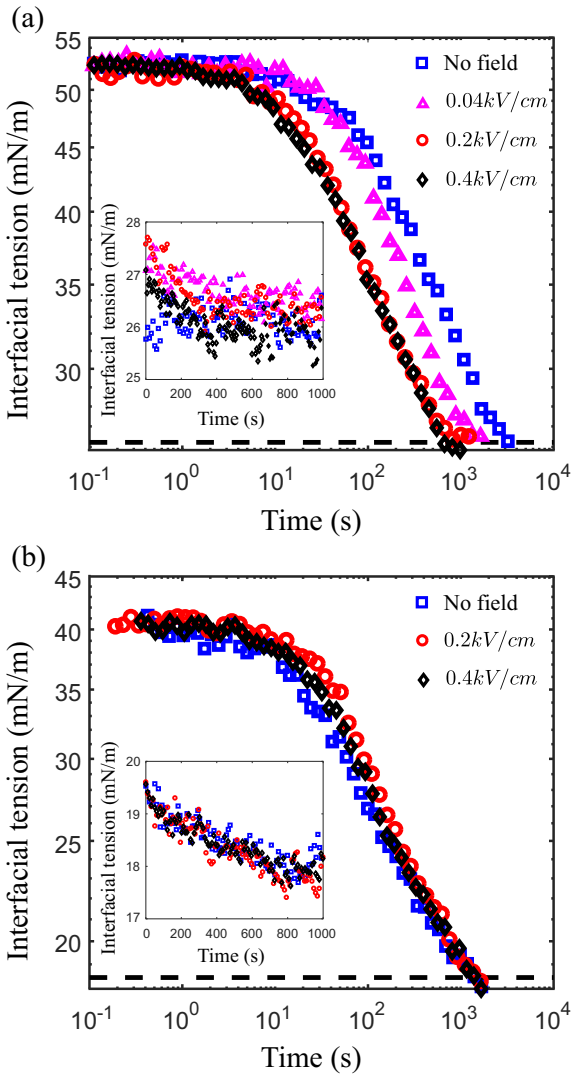

FIG. 2. Dynamic interfacial tension for (a) 4 μM OLOA 11000 in Isopar-M and (b) 10 μM Pluronic L64 in 100 cSt silicone oil. The dashed line represents the steady-state interfacial tension. Inset: Dynamic interfacial tension for each system during the last 1000 s under each electric field. The time axis has been shifted so that all the curves fit in the same time range of 0 to 1000 s.

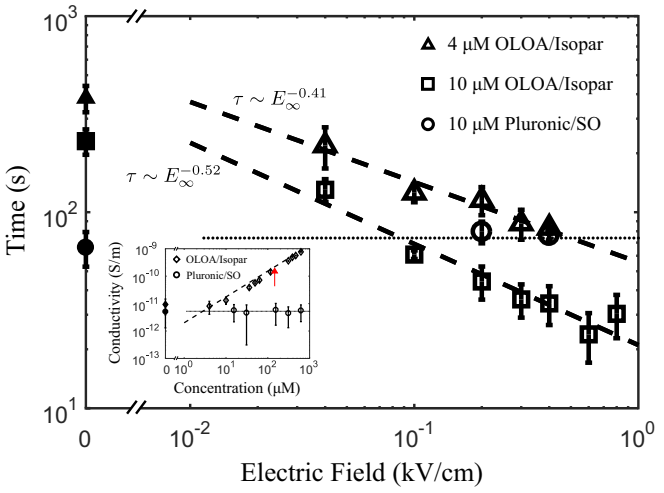

FIG. 3. Time required for the oil-water interface to reach an interfacial tension of 35 mN/m for OLOA 11000 in Isopar-M and 30 mN/m for Pluronic L64 in silicone oil as a function of electric field. The dashed lines represent power-law scalings for OLOA in Isopar-M. The horizontal dotted line establishes that the timescale is independent of field strength for Pluronic in silicone oil. The filled symbols denote the timescale under zero electric field. Inset: Electrical conductivity as a function of surfactant concentration. The arrow shows the CMC of OLOA 11000 in Isopar-L [41]. The dashed line shows the linear dependence of conductivity with concentration for OLOA in Isopar-M. The dotted horizontal line shows that the conductivity of Pluronic in silicone oil is independent of surfactant concentration. The filled symbols denote the conductivity of pure oils, without externally added surfactant.

In contrast, the transport of Pluronic to the silicone oil-water interface was not influenced by the electric field Figure 2(b)]. For a 10 μM system, the interfacial tension relaxes from the clean value and approaches steady state. Even at the highest value of the field strength, the dynamic interfacial tension curve overlaps the curve obtained in the absence of a field. As shown in the inset, the interfacial tension did not completely relax to a steady-state value; however, the slope of the curves flattens out, suggesting that the system approaches steady state. Since the curves overlap each other throughout the experiment, we conclude that, similarly to the OLOA system, the steady-state interfacial tension is unaltered by the electric field.

As a measure of the effect of electric field on surfactant transport, we plot the time required for the interfacial tension to relax from the clean value to a specific value, γ_t, for each system as a function of the field strength. For OLOA in Isopar, we choose $\gamma_t = 35$ mN/m and for Pluronic in silicone oil $\gamma_t = 30$ mN/m. These values are chosen because they are roughly half the value of the interfacial tension of the pure oil-water interface and the steady-state interfacial tension at the given surfactant concentration. For low bulk surfactant concentrations, as has been chosen in this study, a specific value of interfacial tension physically corresponds to the interface reaching a specific surfactant coverage. The result is shown in Fig. 3. For the OLOA system, this timescale follows a power-law scaling, with the exponents 0.41 and 0.52 for the 4 μM and 10 μM systems, respectively. The 10 μM system reaches the same surfactant coverage faster than the 4 μM system at all field strengths, in agreement with previous observations of faster diffusion from a more concentrated bulk solution to an interface [35]. The power-law scaling with electric field is analogous to the effect of bulk phase convection on surfactant transport to fluid-fluid interfaces, rendered rigid due to large gradients in interfacial surfactant concentration [36]. Convection in the continuous phase reduces the effective boundary layer thickness for mass transport of the surfactant, thus the timescale for the surfactant to diffuse from the bulk to the interface reduces. For Pluronic in silicone oil, the timescale does not change on the application of an electric field, as is shown by the dotted line.

The observed phenomena can be explained from the measurement of the electrical conductivity of surfactant doped oils as a function of surfactant concentration, shown in the inset of

Fig. 3. The conductivity was measured using a nonaqueous conductivity probe, DT 700 (Dispersion Technology). For OLOA, the conductivity increases linearly, while for Pluronic, the conductivity does not change with surfactant concentration. The CMC of OLOA 11000 in Isopar-L is reported to be around 140 μM [41] and is shown by the arrow in the inset. Assuming a similar CMC in Isopar-M, it follows that the conductivity of the oil increases both above and below the CMC, implying the presence of charged species even at concentrations below the CMC. Analogously to a previous study, we hypothesize that OLOA forms charged complexes with ionic impurities present in Isopar below the CMC [40].

The surfactant complex experiences an electric force qE_∞, where q is the charge of the complex. It moves with an electrophoretic velocity, $U_E = qE_\infty/6\pi\mu_o l$, where μ_o is the viscosity of the oil, and l is the characteristic linear dimension of the complex. Assuming that q is equal to the charge of one electron, and the typical size of surfactant molecules $l \approx 5$ nm [45], $U_E \approx 5 \times 10^{-3}$–$5 \times 10^{-2}$ mm/s under the field strengths studied. For diffusion to spherical interfaces, the length scale for diffusion, h_s, depends on the radius of curvature of the interface, bulk concentration, and isotherm [34]. We do not measure the equilibrium isotherm of OLOA at the Isopar-water interface, however, using typical parameter values of equilibrium surfactant coverage for surfactants at oil-water interfaces [44] and the radii and bulk concentrations used in this study, $h_s \approx 0.35$–3.5 mm. The timescale for the surfactant complex to migrate this distance under an electric field is $\tau_E = h_s/U_E \approx 7$–$700$ s. The diffusion timescale is given by $\tau_d = h_s^2/D$, where D is the diffusion coefficient. For the dilute bulk surfactant concentrations chosen in this study ($\leqslant 5 \times 10^{-4}$ wt %), we assume that the surfactant complexes do not interact with each other and estimate D using the Stokes-Einstein equation, $D = k_B T/6\pi\mu_o l$, k_B, and T being the Boltzmann constant and temperature, respectively [46]. Using this, we estimate $\tau_d \approx 3.8 \times 10^3$–$3.8 \times 10^5$ s. An electric Pectlet number can be calculated as the ratio of the diffusion to electrophoretic timescale, $\mathrm{Pe}_E = qE_\infty h_s/k_B T$. For the field strengths used in this study, $\mathrm{Pe}_E \sim 55$–5500. Even at the smallest field, electrophoretic migration is faster than diffusion. This manifests as an enhanced transport to the interface. Although a more rigorous analysis involving an investigation of the dependence of h_s on E_∞, and measurement of charge on the complex is required to explain the power-law coefficient, the migration of charged surfactant complexes under electric fields at timescales faster than the diffusion time qualitatively explains the results.

The Pluronic surfactant does not acquire charge in silicone oil, and hence will not experience electrophoretic migration under an electric field. The conductivity difference between the silicone oil and water is huge: $\sim\mathcal{O}(10^6)$. As a consequence, the tangential electric stresses at the interface is negligible, eliminating any electrohydrodynamic flow. Surfactant motion due to dielectrophoresis is nearly $\mathcal{O}(10^{-3})$ slower than diffusion. Hence, the transport of Pluronic to silicone oil-water interface is not influenced by the applied field.

The surfactant transport can be precisely controlled by temporal variation of the field. This is demonstrated in Fig. 4 for 4 μM OLOA in Isopar. We performed an experiment which started under no external field. A field of 0.2 kV/cm

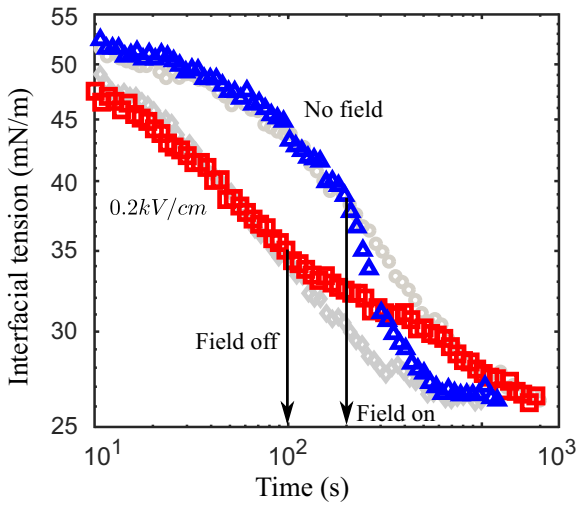

FIG. 4. Dynamic interfacial tension for 4 μM OLOA 11000 in Isopar-M at zero electric field (○), 0.2 kV/cm (◇), from zero field to 0.2 kV/cm at 200 s (△), and from 0.2 kV/cm to zero field at 100 s (□). The arrows indicate the time when the field was switched off or on.

was applied at 200 s, before steady state was reached. The transport dynamics changes at the instant the field is turned on, and the dynamic interfacial tension curve shifts from the curve obtained under zero field (for all times) to the curve obtained under 0.2 kV/cm (for all times). Another experiment was performed, which started under a field of 0.2 kV/cm, with the field switched off at 100 s. Again, the dynamics changes instantaneously with the field being turned off, and the curve shifts to the one obtained under zero field. Similar control and precision was observed in experiments performed at other field strengths, and for 10 μM OLOA, confirming that this is a robust phenomena. Note that Fig. 4 shows data 10 s after a new interface was formed; hence the curves do not start from the same value of interfacial tension.

For all experiments where the field was turned on at some point before steady state, the time to shift from the curve under zero field to the curve under an applied field is around 100 s. This is comparable to the electrophoretic time, τ_E, assuming $h_s \sim 1$ mm, reaffirming that surfactant migration due to electrophoresis is likely responsible for this phenomenon. The timescale to move from the curve under an applied field to a curve under zero field is significantly smaller than the diffusion time assuming $h_s \approx 1$ mm.

Experiments performed with the direction of the electric field reversed showed the same effect as shown in Figs. 2 and 4. This is expected because the interface is radially symmetric. Further, assuming disproportionation to be the charging mechanism, an equal number of positively and negatively charged surfactant complexes will be formed. Hence, the transport will be enhanced, regardless of the direction of the electric field.

The phenomena observed in this work would be difficult to capture in a pendant drop apparatus, which is traditionally used to measure surfactant transport to fluid-fluid interfaces. That technique requires millimeter size interfaces to accurately measure the dynamic interfacial tension. At such length scales $\mathrm{Ca}_E \approx 0.1$, resulting in significant deformation or even

electric field–induced instability of the interface. This will significantly reduce the range of field strength that can be studied in such devices. Further, the timescale for adsorption to millimeter size interfaces is nearly an order of magnitude slower than to the microscale interfaces used here [35]; hence a significantly longer experiment would be needed to capture any effect. Although bulk phase convection has been observed to enhance surfactant transport [36] akin to electric fields, the "on-off" experiments shown in Fig. 4 are more precise due to the instantaneous scheduling of the electric fields.

IV. CONCLUSIONS

We have reported robust experiments to demonstrate electric fields as a new parameter to precisely manipulate the rate of surfactant transport to microscale oil-water interfaces. This phenomena should be generic to oil-soluble surfactants which form charge carriers. The field enhanced transport could enable new tools for controlled electrocoalescence of drops in nonpolar media or laboratory-on-chip methods for droplet manipulation in microfluidic devices.

ACKNOWLEDGMENTS

We are grateful for support by the National Science Foundation through Grant No. CBET-1804548, and partial support by the John E. Swearingen Graduate Fellowship, and the Bushnell Fellowship to R.S.

[1] M. Goto, J. Irie, K. Kondo, and F. Nakashio, Electrical demulsification of w/o emulsion by continuous tubular coalescer, J. Chem. Eng. Jpn. **22**, 401 (1989).

[2] S. Mhatre, V. Vivacqua, M. Ghadiri, A. Abdullah, M. Al-Marri, A. Hassanpour, B. Hewakandamby, B. Azzopardi, and B. Kermani, Electrostatic phase separation: A review, Chem. Eng. Res. Des. **96**, 177 (2015).

[3] B.-J. De Gans, P. C. Duineveld, and U. S. Schubert, Inkjet printing of polymers: State of the art and future developments, Adv. Mater. **16**, 203 (2004).

[4] J.-U. Park, M. Hardy, S. J. Kang, K. Barton, K. Adair, D. Kishore Mukhopadhyay, C. Y. Lee, M. S. Strano, A. G. Alleyne, J. G. Georgiadis, P. M. Ferreira, and J. A. Rogers, High-resolution electrohydrodynamic jet printing, Nat. Mater. **6**, 782 (2007).

[5] T. C. Scott and W. G. Sisson, Droplet size characteristics and energy input requirements of emulsions formed using high-intensity-pulsed electric fields, Sep. Sci. Technol. **23**, 1541 (1988).

[6] T. C. Scott, D. W. DePaoli, and W. G. Sisson, Further development of the electrically driven emulsion-phase contactor, Ind. Eng. Chem. Res. **33**, 1237 (1994).

[7] R. B. Karyappa, A. V. Naik, and R. M. Thaokar, Electroemulsification in a uniform electric field, Langmuir **32**, 46 (2015).

[8] K. Ahn, J. Agresti, H. Chong, M. Marquez, and D. A. Weitz, Electrocoalescence of drops synchronized by size-dependent flow in microfluidic channels, Appl. Phys. Lett. **88**, 264105 (2006).

[9] C. Priest, S. Herminghaus, and R. Seemann, Controlled electrocoalescence in microfluidics: Targeting a single lamella, Appl. Phys. Lett. **89**, 134101 (2006).

[10] D. R. Link, E. Grasland-Mongrain, A. Duri, F. Sarrazin, Z. Cheng, G. Cristobal, M. Marquez, and D. A. Weitz, Electric control of droplets in microfluidic devices, Angew. Chem. Int. Edit. **45**, 2556 (2006).

[11] P. He, H. Kim, D. Luo, M. Marquez, and Z. Cheng, Low-frequency ac electro-flow-focusing microfluidic emulsification, Appl. Phys. Lett. **96**, 174103 (2010).

[12] G. I. Taylor, Studies in electrohydrodynamics. i. The circulation produced in a drop by electrical field, Proc. R. Soc. London. Ser. A **291**, 159 (1966).

[13] J. Sherwood, Breakup of fluid droplets in electric and magnetic fields, J. Fluid Mech. **188**, 133 (1988).

[14] D. Saville, Electrohydrodynamics: The Taylor-melcher leaky dielectric model, Ann. Rev. Fluid Mech. **29**, 27 (1997).

[15] E. Lac and G. Homsy, Axisymmetric deformation and stability of a viscous drop in a steady electric field, J. Fluid Mech. **590**, 239 (2007).

[16] R. T. Collins, J. J. Jones, M. T. Harris, and O. A. Basaran, Electrohydrodynamic tip streaming and emission of charged drops from liquid cones, Nat. Phys. **4**, 149 (2008).

[17] R. T. Collins, K. Sambath, M. T. Harris, and O. A. Basaran, Universal scaling laws for the disintegration of electrified drops, Proc. Natl. Acad. Sci. USA **110**, 4905 (2013).

[18] J. A. Lanauze, L. M. Walker, and A. S. Khair, Nonlinear electrohydrodynamics of slightly deformed oblate drops, J. Fluid Mech. **774**, 245 (2015).

[19] D. Das and D. Saintillan, Electrohydrodynamics of viscous drops in strong electric fields: numerical simulations, J. Fluid Mech. **829**, 127 (2017).

[20] Y. Mori and Y.-N. Young, From electrodiffusion theory to the electrohydrodynamics of leaky dielectrics through the weak electrolyte limit, J. Fluid Mech. **855**, 67 (2018).

[21] P. M. Vlahovska, Electrohydrodynamics of drops and vesicles, Annu. Review of Fluid Mech. **51**, 305 (2019).

[22] J.-W. Ha and S.-M. Yang, Effect of nonionic surfactant on the deformation and breakup of a drop in an electric field, J. Colloid Interf. Sci. **206**, 195 (1998).

[23] J. S. Raut, S. Akella, A. K. Singh, and V. M. Naik, Catastrophic drop breakup in electric field, Langmuir **25**, 4829 (2009).

[24] K. E. Teigen and S. T. Munkejord, Influence of surfactant on drop deformation in an electric field, Phys. Fluids **22**, 112104 (2010).

[25] H. Nganguia, Y.-N. Young, P. M. Vlahovska, J. Blawzdziewicz, J. Zhang, and H. Lin, Equilibrium electro-deformation of a surfactant-laden viscous drop, Phys. Fluids **25**, 092106 (2013).

[26] J. A. Lanauze, R. Sengupta, B. J. Bleier, B. A. Yezer, A. S. Khair, and L. M. Walker, Colloidal stability dictates drop breakup under electric fields, Soft Matter **14**, 9351 (2018).

[27] C. Sorgentone, A.-K. Tornberg, and P. M. Vlahovska, A 3d boundary integral method for the electrohydrodynamics of surfactant-covered drops, J. Comput. Phys. **389**, 111 (2019).

[28] S.-Y. Lin, K. McKeigue, and C. Maldarelli, Diffusion-controlled surfactant adsorption studied by pendant drop digitization, AIChE J. **36**, 1785 (1990).

[29] R. Pan, J. Green, and C. Maldarelli, Theory and experiment on the measurement of kinetic rate constants for surfactant exchange at an air/water interface, J. Colloid Interf. Sci. **3205**, 213 (1998).

[30] S.-Y. Lin, R.-Y. Tsay, L.-W. Lin, and S.-I. Chen, Adsorption kinetics of $C_{12}E_8$ at the air–water interface: adsorption onto a clean interface, Langmuir **12**, 6530 (1996).

[31] J. Eastoe and J. Dalton, Dynamic surface tension and adsorption mechanisms of surfactants at the air-water interface, Adv. Colloid Interfac. **85**, 103 (2000).

[32] T. Svitova, M. Wetherbee, and C. Radke, Dynamics of surfactant sorption at the air/water interface: continuous-flow tensiometry, J. Colloid Interf. Sci. **261**, 170 (2003).

[33] V. Fainerman, S. Lylyk, J. K. Ferri, R. Miller, H. Watzke, M. Leser, and M. Michel, Adsorption kinetics of proteins at the solution/air interfaces with controlled bulk convection, Colloid. Surface. A **282-283**, 217 (2006).

[34] N. J. Alvarez, L. M. Walker, and S. L. Anna, Diffusion-limited adsorption to a spherical geometry: The impact of curvature and competitive time scales, Phys. Rev. E **82**, 011604 (2010).

[35] N. J. Alvarez, L. M. Walker, and S. L. Anna, A microtensiometer to probe the effect of radius of curvature on surfactant transport to a spherical interface, Langmuir **26**, 13310 (2010).

[36] N. J. Alvarez, D. R. Vogus, L. M. Walker, and S. L. Anna, Using bulk convection in a microtensiometer to approach kinetic-limited surfactant dynamics at fluid-fluid interfaces, J. Colloid Interf. Sci. **372**, 183 (2012).

[37] V. Novotny, Applications of nonaqueous colloids, Colloids Surf. **24**, 361 (1987).

[38] I. D. Morrison, Electrical charges in nonaqueous media, Colloids Surf. A **71**, 1 (1993).

[39] B. A. Yezer, A. S. Khair, P. J. Sides, and D. C. Prieve, Determination of charge carrier concentration in doped nonpolar liquids by impedance spectroscopy in the presence of charge adsorption, J. Colloid Interf. Sci. **469**, 325 (2016).

[40] Q. Guo, V. Singh, and S. H. Behrens, Electric charging in nonpolar liquids because of nonionizable surfactants, Langmuir **26**, 3203 (2009).

[41] M. Gacek, D. Bergsman, E. Michor, and J. C. Berg, Effects of trace water on charging of silica particles dispersed in a nonpolar medium, Langmuir **28**, 11633 (2012).

[42] M. D. Reichert and L. M. Walker, Coalescence behavior of oil droplets coated in irreversibly-adsorbed surfactant layers, J. Colloid Interface Sci. **449**, 480 (2015).

[43] S. M. Kirby, S. L. Anna, and L. M. Walker, Sequential adsorption of an irreversibly adsorbed nonionic surfactant and an anionic surfactant at an oil/aqueous interface, Langmuir **31**, 4063 (2015).

[44] N. J. Alvarez, W. Lee, L. M. Walker, and S. L. Anna, The effect of alkane tail length of cie8 surfactants on transport to the silicone oil–water interface, J. Colloid Interface Sci. **355**, 231 (2011).

[45] B. A. Yezer, A. S. Khair, P. J. Sides, and D. C. Prieve, Use of electrochemical impedance spectroscopy to determine double-layer capacitance in doped nonpolar liquids, J. Colloid Interface Sci. **449**, 2 (2015).

[46] C. C. Miller, The stokes-einstein law for diffusion in solution, Proc. R. Soc. Lond. A **106**, 724 (1924).